Positive-Contrast Imaging of Microscopic Paramagnetic Particles using Field-Encoded Fluctuating-Equilibrium SSFP

W. R. Overall[1], and J. M. Pauly[1]

[1]Stanford University, Stanford, CA, United States

Introduction: Positive-contrast techniques for visualizing paramagnetic agents (e.g., SPIO particles) attempt to maximize signal from areas near the agent while completely suppressing other spins. For these techniques to be useful in cellular and molecular imaging applications, small quantities of agent must be reliably detectable within inhomogeneous tissues. Existing methods [1-4] select marker signals through either their induced field shift or the local gradients they generate. We propose a new technique that is selective along both of these axes for improved suppression robustness [3] while allowing the flexibility for 2D slice-selective RF pulses. The technique uses a fluctuating-equilibrium (FEMR) [5] steady state to provide spectral selection, which provides excellent SNR efficiency while allowing a fully registered anatomic image to be acquired concurrently. Furthermore, the short echo time minimizes diffusion losses that limit detection efficiency in other techniques. Through simulations and *ex vivo* validation, we demonstrate the applicability of the technique for imaging nanogram quantities of SPIO in tissues.

Methods: The pulse sequence, which we call field-encoded fluctuating-equilibrium SSFP (Fe^2-SSFP), uses balanced gradients and 0^o-90^o RF phase cycling to generate two echoes (Fig. 1a). Frequencies are set such that on-resonant water is alternately preserved and suppressed in adjacent echoes (Fig. 1b). If TR is chosen appropriately (4.6ms at 1.5T), fat signals alternate similarly. In the water-suppressed Echo 1, equal and opposite rephasing gradients are added on either side of the readout to further select signal based on its local gradient. Such gradients rephase spins in areas of large local gradient near paramagnetic markers, and dephase signals from other areas [3]. This approach is insensitive to bulk field inhomogeneity, but is known to fail near high-spatial-frequency edges. Rephasing gradients are omitted in the water-preserving Echo 2 to provide a registered anatomic reference image with contrast similar to that of balanced SSFP.

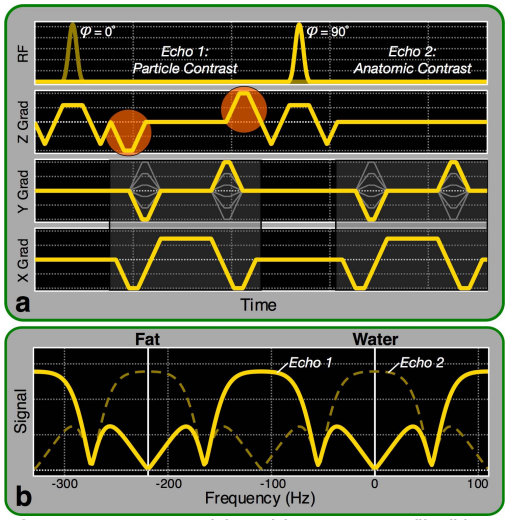

Figure 1: *Sequence (a) and frequency profile (b). A 0^o-90^o phase cycling scheme produces two echoes with alternating spectral sensitivity. Echo 1 has low on-resonant signal, and rephasing gradients (orange) are added to further suppress regions with low local gradients. Echo 2 is not altered, and therefore exhibits SSFP-like anatomic contrast.*

Simulations were implemented to analyze the linearity and detection limits of the technique under typical imaging conditions. Phantom experiments were performed at 1.5T with TR=4.6ms, TE=1.8ms, 30^o tip, NEX=16, 16-cm FOV, 256^2 matrix, 8-mm slice thickness, and through-plane rephasing-gradient area of 7.5 cyc/cm. Total imaging time was less than 40 seconds. A gel phantom composed of 4% agar doped with 8 mM $NiCl_2$ and 1µl/l BioMag SPIO solution (Bangs Laboratories, Fishers, IN; 10.5-µm mean particle size) was used to test sequence performance for small particles. Further images were collected in an *ex vivo* pork sample after a 0.1-µl injection of BioMag particles to verify the technique's ability to suppress high-spatial-frequency structures and fat. White-marker [4] and negative-contrast GRE (TR=20ms; TE=17ms) images were acquired for comparison.

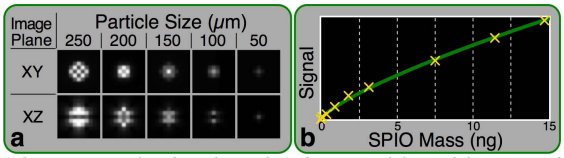

Figure 2: *Simulated marker images (a) and integrated signal vs. SPIO mass (b). Signal increase is nearly linear with particle mass and correlates well with theory (green).*

Results: Simulated Fe^2-SSFP images (Fig. 2a) show the theoretical positive-contrast signal arising from a range of particle sizes. Signal distribution varies depending on the relative orientations of the imaging plane and rephasing-gradient axis, but in all cases extends to a radius more than 10x that of the particle. Total integrated signal increases with SPIO mass (Fig. 2b) and closely matches Signal $\propto$ $Mass^{3/4}$, a nearly linear relationship that can be derived analytically.

Images from the agar phantom show excellent agreement between GRE signal voids (Fig. 3a) and areas of positive contrast using our technique (Fig. 3b). Apparent particle sizes vary from 20-200 µm. The smallest visible particles correlate well with simulated values for SPIO volumes around .5 nanogram, or approximately fifty BioMag particles. Images from the pork sample matched well with theory (Fig. 4a-c), and demonstrated excellent background suppression in the presence of lipid and high-spatial-frequency structures. By comparison, the standard white-marker technique provided lower marker signal and background leakage greatly reduced marker conspicuity (Fig. 4d).

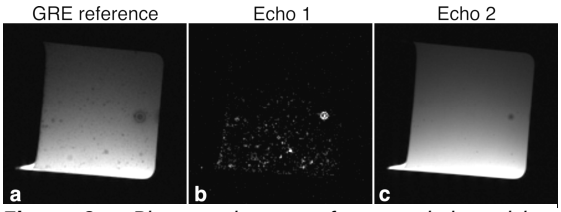

Figure 3: *Phantom images of suspended particles. Negative-contrast GRE (a) shows marker locations, which correlate well with positive-contrast locations (b) from Echo 1 of our technique. Echo 2 (c) shows conventional SSFP contrast with minimal marker-signal loss.*

Discussion: We have developed a new technique that can provide positive-contrast visualization of paramagnetic agents. By combining spectral and gradient-based suppression, background signals are more robustly rejected than would be possible using either approach alone. Initial experiments demonstrate adequate background suppression for the visualization of microscopic quantities of iron oxides, even in the presence of high-frequency background structures or field inhomogeneities. Further research is required to determine the limits of detection of the technique in cell media.

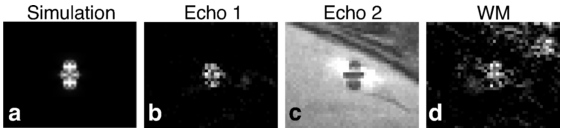

Figure 4: *Cropped images from a pork sample. Simulated Fe^2-SSFP signal (a) corresponds well with the acquired Echo 1 (b) for the injected volume of 0.1µl. Echo 2 (c) shows negative contrast. An image acquired with the white-marker technique (d) has lower marker signal and does not adequately suppress background.*

References: [1]. Seppenwoolde JH, *et al*. MRM 50(4): 784-790, 2003.

[2]. Cunningham CH, *et al*. MRM 53(5): 999-1005, 2005.

[3]. Overall WR, *et al*. Proc. 15th ISMRM: 579, 2007.

[4]. Lau AZ, *et al*. Proc. 15th ISMRM: 1225, 2007.

[5]. Vasanawala SS, *et al*. MRM 42(5): 876-883, 1999.